Neutral pH Plasma-Activated Water eliminates ESKAPE pathogens via reactive nitrogen species with dual potential for surface sanitation and wound cleansing

Debapriya Mukherjee[1#], Pallab Ghosh[1#], Atish Roy Chowdhury[1], Nishanth Vishwa[2], Kavita Verma[2], Lakshminarayana Rao[*2], Dipshikha Chakravortty[*1,3]

1 Department of Microbiology and Cell Biology, Indian Institute of Science, Bangalore, India

2 Centre for Sustainable Technologies, Indian Institute of Science, Bangalore, India

2 Interdisciplinary Centre for Water Research, Indian Institute of Science, Bangalore, India

3 School of Biology, Indian Institute of Science Education and Research, Thiruvananthapuram, India

 # Equal contribution

*** Corresponding Authors**

Lakshminarayana Rao, Centre for Sustainable Technologies, Indian Institute of Science, Bangalore, Karnataka 560012, India.

Email: narayana@iisc.ac.in

Dipshikha Chakravortty, Department of Microbiology and Cell Biology, Indian Institute of Science, Bangalore, Karnataka 560012, India.

Email: dipa@iisc.ac.in

Abstract

Plasma-activated water (PAW) is an emerging antimicrobial strategy, though its efficacy has traditionally depended on acidic pH to generate reactive species. To improve clinical and practical applicability, we developed a neutral pH formulation using buffered water—hs-PAbW—and evaluated its antimicrobial activity and mechanism of action against ESKAPE pathogens. hs-PAbW significantly reduced bacterial viability during the exponential growth phase. While reactive oxygen species (ROS) alone were insufficient for bacterial killing, reactive nitrogen species (RNS), particularly peroxynitrite, mediated strong microbicidal effects via nitrotyrosine formation. These effects occurred independently of acidic conditions, demonstrating that antimicrobial activity is retained at neutral pH. Alongside, hs-PAbW effectively reduced bacterial burden on metal surfaces and exhibited superior killing compared to high doses of standard antibiotics, including ceftazidime, ciprofloxacin, and meropenem *in vitro*. A non-cytotoxic dose of hs-PAbW also reduced bacterial load in infected wounds and accelerated wound closure *in vivo*. These findings highlight the dual functionality of hs-PAbW in surface sanitation and wound care, and support its potential as a sustainable, broad-spectrum antimicrobial agent for clinical use.

Keywords: Plasma-activated water (hs-PAbW), reactive oxygen species (ROS), reactive nitrogen species (RNS), peroxynitrite, ESKAPE pathogens, enteropathogen, antibiotics.

Introduction

Antimicrobial resistance (AMR) is recognized by the World Health Organization as a critical global health threat, with over two million antibiotic-resistant infections and 23,000 related deaths annually in the US alone[1, 2]. Globally, bacterial AMR caused 1.27 million deaths in 2019[3]. *Acinetobacter*, *Pseudomonas,* and non-typhoidal *Salmonella* are a few of the bacterial pathogens which are predominantly associated with AMR-related deaths [1, 3, 4]. This is why developing a novel, long-lasting, and sustainable solution for bacterial infections remains a significant necessity.

Plasma-activated water (PAW) is an emerging technology that has gained attention for its potential as a sustainable solution to various medical and food preservation applications [5-7]. PAW is produced by exposing water to cold plasma, an ionized gas containing charged particles like ions, electrons, and neutral atoms [8]. The ionized particles in the plasma interact with the water molecules generating reactive oxygen species (ROS) and reactive nitrogen species (RNS) [9]. These ROS and RNS generated have varying lifetimes, ranging from a few nanoseconds to a few years [10, 11]. Various applications of PAW such as anti-cancer [7], antimicrobial [12], anti-viral [13], food preservation [5, 14], insecticidal [15], oral hygiene [16, 17] and anti-fungal [18] have been demonstrated by various researchers. These studies have mostly worked with acidic pH PAW [10, 18, 19]. However, the acidic pH of a solution can contribute to its corrosiveness, limiting its practical use, as prolonged exposure may accelerate the degradation of metals like stainless steel [20].

Real-world application of PAW requires the generation of neutral pH PAW, which has been successfully designed by our group before [21, 22]. In this study, we highlight the bactericidal efficacy and mode of action of neutral-pH hs-PAbW (pH 7–7.4) against ESKAPE pathogens, which can cause pneumonia, surgical site, and bloodstream infections [23, 24]. Demonstrating that

hs-PAbW retains bactericidal activity at neutral pH enhances its physiological relevance, supporting its application in metal surface disinfection and wound cleansing to prevent hospital-acquired ESKAPE infections.

Materials and Methods

Generation of hs-PAbW, ROS-PAW, RNS-PAbW

We have generated hs-PAbW, ROS-PAW, RNS-PAbW by the protocol as described before. To maintain parity with our previous study, we have used the nomenclature hs-PAbW and RNS-PAbW as both have been generated using buffered water [21].

Briefly, hs-PAbW, ROS-PAW, and RNS-PAbW were generated using a 10 kV, 20 kHz AC plasma discharge in a 100 ml glass bottle with aluminium electrodes, treating 50 ml of liquid for 60 minutes, repeated at least three times. hs-PAbW, containing both ROS and RNS, was produced using 25 mM bicarbonate water with 1 LPM air bubbling and a 5 mm discharge, consuming 32 ± 2 W. ROS-PAW was generated from demineralized water with 1 LPM argon bubbling, a 5 mm discharge, and an ice jacket to prevent overheating, consuming 38 ± 2 W. RNS-PAbW was produced from 25 mM bicarbonate water with 1 LPM air bubbling and a 5 mm discharge, without an ice jacket, consuming 32 ± 2 W **(Figure 1A)**.

Bacterial strains and sample preparation

Methicillin Resistant *Staphylococcus aureus* (Isolate-SA3), hyper viscous (hv) *Klebsiella pneumoniae* (pus isolate 529) [22] (*S. aureus* and *K. pneumoniae* were kind gifts from Prof. Pradyut Prakash, Benaras Hindu University, India)[25], *Acinetobacter baumannii* strain S2 (ATCC), and *Pseudomonas aeruginosa* PAO1 (a generous gift from Prof. Anne-Béatrice Blanc-Potard, Université de Montpellier) were revived on Luria- Bertani (LB) agar plates without

92 antibiotics from glycerol stock stored at -80^0 C. One colony was inoculated in the LB broth and
93 grown overnight in a shaking incubator (170 rpm) at 37^{0}C. After 12 hours, the stationary phase
94 bacteria were subcultured (1:100) into freshly prepared LB broth and incubated for 4 to 5 hours
95 to obtain the exponential growth phase. The $(OD)_{600}$ of the bacterial cultures were adjusted to
96 0.3 (~10^8 CFU/ mL) and 0.1 (~10^6 CFU/ mL), respectively, centrifuged and the pellet was
97 resuspended in 1 ml of control water, hs-PAbW, ROS-PAW, RNS-PAbW, and antibiotic
98 solutions with high concentration (50 µg/ mL) of ceftazidime, ciprofloxacin, and meropenem
99 for 45 minutes.

100

101

102 **Bacterial spread plating**

103 Exponential-phase bacterial pellets of *S. aureus*, *K. pneumoniae*, *P. aeruginosa*, and *A.*
104 *baumannii* were resuspended in 1 ml of water samples and incubated until the designated time
105 points. After incubation, suspensions were serially diluted in 1X PBS, plated on LB agar, and
106 incubated overnight at 37°C. Colony-forming units (CFU) were then recorded.

107

108 **Flow cytometry analysis.**

109 Bacterial pellets from exponential-phase cultures of *S. aureus*, *K. pneumoniae*, *A. baumannii*,
110 and *P. aeruginosa* were incubated in 1 ml of control water, hs-PAbW, ROS-PAW, RNS-PAbW,
111 or an antibiotic solution for 45 minutes. After centrifugation (6000 rpm, 10 min) and washing,
112 cells were resuspended in 1 ml of double-autoclaved milli-Q water. To measure reactive
113 nitrogen species, diaminofluorescein-2 diacetate (DAF_2DA, 10 µM) was added and incubated
114 for 30 minutes (excitation: 491 nm, emission: 513 nm) [26]. Similarly, treated cells were

115 incubated with dichlorodihydrofluorescein diacetate (DCF_2DA, 10 μM) for reactive oxygen
116 species, propidium iodide (PI, 1 μg/mL) for bacterial death, and $DiBAC_4$ (1 μg/mL) for
117 membrane depolarization. Samples were analysed via flow cytometry (BD FACSVerse, BD
118 Biosciences), and data were processed using BD FACSuite software [27]. Representative dot
119 plots indicate the percentage of positive values.

120

121 **Scanning Electron Microscopy**

122 Bacterial pellets from exponential cultures of *S. aureus*, *K. pneumoniae*, *P. aeruginosa*, *A.*
123 *baumannii* were resuspended in 1 ml of the water samples. Post incubation of 45 mins, they
124 were drop-casted on clear glass coverslips and air-dried. The samples were fixed by using 3.5%
125 glutaraldehyde overnight at 4˚C. The next day, they underwent a sequential dehydration process
126 using 10%, 30%, 50%, 70%, 90%, and 100% alcohol, with each treatment lasting 3 minutes.
127 The samples were dried using a vacuum- desiccator and subjected to gold spluttering before
128 imaging. Thermofischer XL-30 ESEM was used for all the image acquisition at a magnification
129 of 5000X. Bacteria on the metal surface were visualized using JEOL SEM IT-300 at the same
130 magnification.

131

132 **Peroxynitrite Estimation Assay**

133 The intracellular peroxynitrite assay was performed using Peroxynitrite Assay Kit from Abcam
134 (ab2334690), using manufacturer's protocol. Briefly, cell pellets from the exponential phase
135 cultures of the tested pathogens were incubated in 1 ml of all the water samples for 45 minutes.
136 Following this, the cells were centrifuged at 6,000 rpm for 10 minutes and the pellet was
137 resuspended in fresh milliQ. 50 µl of the cell suspension was incubated with 50 µl of the

138 reaction mix for 20 minutes. Following this, the fluorescence intensities were measured using
139 a Tecan microplate reader, with Ex/Em at 490/530 nm.

140

141 **Atomic Force Microscopy**

142 Bacterial pellets from exponential phase cultures of *S. aureus* and *K. pneumoniae* were
143 resuspended in 1 ml of each water sample. After 45 minutes of incubation, the bacterial
144 suspensions were centrifuged again at 6,000 rpm for 10 minutes, and the pellets were fixed
145 using 3.5% paraformaldehyde. The bacterial suspensions were diluted 100-fold and 50 µl
146 aliquot of each diluted sample was drop-cast onto coverslips and allowed to air dry. The images
147 were captured using the NX10 AFM, and the length, height, and Young's modulus of the
148 bacterial cells were measured with XEI software[28].

149

150 **Nitrotyrosine estimation**

151 The pellets from exponential phase cultures of *S. aureus* and *K. pneumoniae* were centrifuged
152 at 6,000 rpm for 10 minutes were resuspended in 1 ml of each water sample. After 45 minutes
153 of incubation, the bacterial cells were lysed via sonication at 30% amplitude with 20-second
154 pulses for a total of 4 minutes. Cell debris was removed by centrifugation at 13,000 rpm for 10
155 minutes at 4˚C. The cell lysate was then concentrated using a speed vac, and protein
156 concentration was determined using the Bradford reagent. An equal amount of protein was used
157 for nitrotyrosine estimation, following the manufacturer's instructions for the Nitrotyrosine
158 ELISA Kit (ab210603) from Abcam. The end product of ELISA was quantified using a Tecan
159 plate reader at 450 nm.

160

161 **Surface sterilisation experiment**

162 Sterile stainless-steel equipment was obtained, and 10^7 CFU of *S. aureus* and *K. pneumoniae*
163 cultures were drop-casted onto the surfaces. After drying for one hour, 200 µl of RNS-PAbW
164 and hs-PAbW were applied to the dried patches and incubated for an additional hour. The water
165 samples were then removed, and the bacteria were resuspended in equal volumes of PBS before
166 being spread plated to determine the CFU count post-exposure. For SEM-assisted bacterial
167 visualization, the samples were fixed with 3.5% glutaraldehyde overnight at 4˚C immediately
168 after water removal. This was followed by dehydration, desiccation, and gold sputtering before
169 imaging, as previously described.

170

171 **MTT Assay**

172 The cytotoxicity of hs-PAbW was assessed using the MTT assay. In brief, L929 mouse
173 fibroblast cells were seeded at a density of 5×10^4 cells per well in a 96-well plate. Once the
174 cells reached 70–80% confluency, they were exposed to varying concentrations of hs-PAbW in
175 a total medium volume of 100 µl and incubated for 24 hours. Following the incubation, the
176 cells were washed with 1× PBS, after which 100 µl of MTT solution (0.5 mg/mL) was added.
177 The plate was then incubated for 4 hours at 37 °C in a CO_2 incubator. Afterward, the cells were
178 treated with 50 µl of dimethyl sulfoxide (DMSO) to dissolve the formazan crystals formed by
179 metabolically active cells. Absorbance was then recorded at 570 nm using a TECAN microplate
180 reader.

181

182 **Ethics statement for animal experiments**

All animal experiments were approved by the Institutional Animal Ethics Committee (IAEC) of the Indian Institute of Science, Bangalore (Registration No. 48/1999/CPCSEA). All procedures were conducted in strict accordance with the guidelines established by the Committee for the Purpose of Control and Supervision of Experiments on Animals (CPCSEA). The ethical clearance number for this study is CAF/Ethics/973/2023.

Wound irrigation experiment

Wound irrigation experiments were performed by adapting previously established protocols [29-31]. Briefly, 10–12-week-old male BALB/c mice were anesthetized intravenously on day 0 using ketamine hydrochloride (120 mg/kg). After dorsal depilation, two full-thickness excisional wounds (10 mm diameter) were created bilaterally along the midline using a sterile biopsy punch. Each wound was inoculated with 10^4 CFU of *S. aureus* and allowed to incubate for 30 minutes before irrigation.

Each wound received 500 µL of the irrigation solutions, applied three times consecutively. Mice were housed individually post-surgery with access to standard diet. Wound irrigation continued alternate days until day 7, with wound images captured throughout the treatment period. On day 7, mice were euthanized, and wound tissues were harvested for bacterial quantification via spread plating on Mannitol Salt Agar (HiMedia). Wound contraction was assessed by measuring wound diameter using ImageJ software.

Statistical Analysis

The number of biological and technical replicates used in each experiment have been reported in the figure legends. The statistical analyses were done by unpaired two-tailed student's t-test,

206 one-way ANOVA, or Mann-Whitney U-test as indicated in the figure legends. The *p* values
207 below 0.05 were considered significant. The results were expressed as mean ± SD or mean±
208 SEM as mentioned in the figure legends. GraphPad Prism 8.4.3 (686) was used to generate the
209 bar graphs and perform the statistical tests.

210

211 ## Results

212 **Plasma-activated water with a neutral pH could eliminate bacteria in the exponential**
213 **growth phase.**

214 We subjected exponential-phase cultures of *Staphylococcus aureus*, *Klebsiella pneumoniae*,
215 *Acinetobacter baumannii*, and *Pseudomonas aeruginosa* to hs-PAbW treatment to evaluate its
216 bactericidal efficacy against these ESKAPE pathogens and determine the minimum exposure
217 time required for its action **(Figure 1B–E)**. hs-PAbW reduced bacterial survival across all
218 species, with varying minimum exposure times: *S. aureus* showed a significant reduction from
219 5 minutes onwards **(Figure 1B)**, *A. baumannii* from 25 minutes onwards **(Figure 1D)**, and
220 hypervirulent *K. pneumoniae* and *P. aeruginosa* started showing immediately **(Figure 1C, E)**.
221 A 45-minute treatment, which significantly reduced viability across all species, was chosen for
222 further experiments. *A. baumannii* and *P. aeruginosa* reached maximum reduction at this point
223 **(Figure 1D, E)**. Survival of *K. pneumoniae* **(Figure 1C)** continued to decrease until 1440
224 minutes, and while *S. aureus* **(Figure 1B)** also showed further reduction, substantial killing
225 was achieved by 45 minutes.

226 To determine whether hs-PAbW also exhibited a bactericidal effect on stationary-phase
227 bacteria, we treated stationary-phase cultures of *S. aureus*, *K. pneumoniae*, *A. baumannii*, and
228 *P. aeruginosa* with hs-PAbW for 45 minutes. The absence of any change in the percentage of
229 propidium iodide (PI)-positive cells indicated that hs-PAbW had no effect on the viability of

230 stationary-phase bacterial cultures **(Figure S1A-S1H)**. From this point forward, exponential-
231 phase cultures were used for all experiments.

232

233 **Unlike the nitrogen species (NO_2^-, NO_3^-) present in hs-PAbW, oxygen species (H_2O_2) alone**
234 **is not capable of independently killing bacterial pathogens.**

235 The microbicidal activity of hs-PAbW can be attributed to its high content of ROS and RNS.
236 We sought to identify the role of each of these functional components in reducing bacterial
237 growth. As we found that hs-PAbW can restrict bacterial growth at the exponential phase, we
238 subjected the exponential phase cultures of all three bacterial strains to the treatment with ROS-
239 PAW **(Figure 2)** and RNS-PAbW **(Figure 3)**.

240 ROS-PAW and RNS-PAbW were prepared to contain ROS and RNS concentrations equivalent
241 to those in hs-PAbW **(Figure 1A)**. ROS-PAW treatment resulted in a higher DCF_2DA-median
242 fluorescence intensity (MFI), indicating elevated ROS levels **(Figure S2A-E).** However, PI
243 staining showed that ROS-PAW was ineffective at killing bacteria despite high intracellular
244 ROS levels **(Figure 2A-F)**. The greater DAF_2DA- MFI value **(Figure S3A-E)** corresponding
245 to RNS-PAbW-treated bacterial cells further showed that treating the bacterial cells with RNS-
246 PAbW generated high concentration of RNS. Unlike ROS-PAW, we observed RNS-PAbW
247 could kill the actively growing bacteria **(Figure 3A-3F)**. Bacterial spread plating confirmed
248 these findings **(Figure S4 A-D)**. DAF_2DA staining of hs-PAbW-treated exponential **(Figure**
249 **S5A-H)** cultures of the test pathogens also showed significantly higher amounts of RNS
250 compared to the control water treatment. Taken together, we could conclude that RNS is the
251 major factor contributing to the microbicidal activity of hs-PAbW (pH=7 to 7.4) in ESKAPE
252 pathogens.

253

254 **High concentration of peroxynitrite in RNS-PAbW and hs-PAbW is one of the factors**
255 **regulating the microbicidal role of hs-PAbW.**

256 Morphological changes were observed in *K. pneumoniae*, *A. baumannii*, and *P. aeruginosa*
257 after hs-PAbW treatment compared to the control **(Figure 4A)**. *K. pneumoniae* exhibited
258 shrinkage, distortion, and clumping, while *A. baumannii* showed visible lysis, and *P.*
259 *aeruginosa* displayed reduced cell size and clumping. ROS-PAW and RNS-PAbW also induced
260 surface morphology changes in all three strains, as seen via SEM. In contrast, *S. aureus* showed
261 no noticeable morphological alterations **(Figure S6)**.

262 Previous studies on *Fusarium graminearum* spores suggested PAW compromises membrane
263 integrity, leading to intracellular content leakage[32]. To investigate this in our samples, we used
264 the membrane-potential-sensitive dye $DiBAC_4$. Results indicated increased membrane
265 depolarization in *P. aeruginosa*, *K. pneumoniae*, and *A. baumannii* **(Figure 4C-E)**, whereas *S.*
266 *aureus* exhibited membrane hyperpolarization **(Figure 4B)**. Although ROS-PAW and RNS-
267 PAbW altered membrane potential, only hs-PAbW demonstrated bactericidal effects,
268 suggesting membrane potential disruption alone is not responsible for its antimicrobial action.

269 We aimed to identify the key chemical species responsible for the bactericidal activity of
270 neutral pH PAW. A significant increase in the PI positive population after RNS-PAbW treatment
271 suggests that RNS in hs-PAbW contribute to its microbicidal effect against ESKAPE
272 pathogens. In addition to ROS and RNS, hs-PAbW contains short-lived species like
273 peroxynitrous acid (ONOOH) and peroxynitrite ($ONOO^-$), which can cause cell damage
274 through direct oxidation or decomposition byproducts[6, 8, 21, 33]. To assess their role, we
275 measured intracellular peroxynitrite levels post-treatment **(Figure 4F-4I)**. While ROS-PAW
276 showed no significant change, RNS-PAbW and hs-PAbW treatments led to a notable increase.
277 In *S. aureus* and *K. pneumoniae* exponential phase culture, RNS-PAbW produced significantly

278 higher peroxynitrite levels than hs-PAbW **(Figure 4F-G)**, whereas in *A. baumannii* and *P.*
279 *aeruginosa*, both treatments generated comparable peroxynitrite levels **(Figure 4H-I)**. This
280 suggests that RNS in hs-PAbW regulate peroxynitrite formation.

281

282 **RNS-PAbW, hs-PAbW, and ROS-PAbW caused a reduction in the length, height, and**
283 **Young's modulus of the Gram-negative bacterium *K. pneumoniae* although ROS-PAW**
284 **was unrelated to increased nitrotyrosine levels in *S. aureus* and *K. pneumoniae***

285 We selected *S. aureus* and *K. pneumoniae* as representative Gram-positive and Gram-negative
286 bacteria, respectively, and analysed their morphological changes using Atomic Force
287 Microscopy **(Figure 5A-F)**. Consistent with SEM data, water sample treatments did not
288 significantly affect *S. aureus* in terms of diameter or Young's modulus **(Figure 5B, C)**.
289 However, *K. pneumoniae* showed a significant reduction in these parameters after exposure to
290 RNS-PAbW, hs-PAbW, and ROS-PAW **(Figure 5D-F).** This suggests that while ROS-PAW
291 does not effectively kill bacteria, it can impact structural integrity, reinforcing that RNS and
292 short-lived species like peroxynitrite, rather than ROS, drive the bactericidal effects of hs-
293 PAbW.

294 Peroxynitrous acid can nitrate both free and protein-bound tyrosine, with 3-nitrotyrosine
295 serving as a biomarker for peroxynitrite formation [34, 35]. This modification can disrupt protein
296 structure and function and is a key defence mechanism in macrophages [36, 37]. In our study,
297 nitrotyrosine was significantly detected in *S. aureus* and *K. pneumoniae* cell lysates after hs-
298 PAbW and RNS-PAbW exposure, indicating active peroxynitrite formation and its
299 antimicrobial role **(Figure 5H)**. As expected, nitrotyrosine was undetectable in bacteria treated
300 with control water and ROS-PAW, reinforcing that RNS and peroxynitrite are crucial for the

301 bactericidal activity of neutral pH hs-PAbW. The standard curve and raw data are provided in
302 supplementary data **(Figure S7)**.

303

304 **hs-PAbW and RNS-PAbW efficiently reduce microbial load on metal surfaces, supporting**
305 **their use as surface disinfectants**

306 Hospital surfaces such as floors and door handles serve as key reservoirs for nosocomial
307 infections, increasing the risk of infection spread both within and beyond the hospital[38, 39].
308 Given the antimicrobial potential of hs-PAbW observed in our previous data, we aimed to
309 explore its potential use as a surface cleansing agent. We used sterile metal surfaces and drop-
310 casted *S. aureus* and *K. pneumoniae* cultures onto them. Both RNS-PAbW and hs-PAbW
311 effectively reduced the bacterial load on metal surfaces after one hour of exposure, as verified
312 by bacterial spread plating **(Figure 6A, B)** and SEM-assisted imaging of infected metal
313 surfaces **(Figure 6C)**, underscoring their potential as a cost-effective surface decontamination
314 solution.

315

316 **Both hs-PAbW demonstrated superior efficacy against ESKAPE pathogens *in vitro***
317 **compared to high-dose antibiotics and effectively reduced bacterial burden in infected**
318 **murine wounds, outperforming commercially available antibiotic**

319 Ceftazidime (third-generation cephalosporin) and meropenem (carbapenem) are β-lactam
320 antibiotics that are routinely used in treating a wide range of MDR bacterial infections [28, 40, 41].
321 Ciprofloxacin is a fluoroquinolone that inhibits the growth of several pathogens by blocking
322 the activity of DNA gyrase (*gyrAB*) [42-44].Since hs-PAbW could successfully reduce the viability
323 of actively growing bacteria, we decided to compare its bactericidal activity with these
324 antibiotics. We harvested bacteria from the exponential phase of their growth and surprisingly,

we observed that hs-PAbW is more effective in inducing bacterial death compared to high concentrations of antibiotics (ceftazidime, ciprofloxacin, and meropenem, concentration- 50 µg/ mL) and hs-PAbW within 45 minutes **(Figure 7A-D)**. The reduced susceptibility of *K. pneumoniae* to meropenem can be overcome by hs-PAbW[45].

To evaluate the suitability of hs-PAbW as a disinfectant, its cytotoxicity was assessed. No significant cytotoxicity was observed up to 20% concentration (**Fig. S8A**). Notably, hs-PAbW retained its antimicrobial activity even when diluted to 20%, effectively reducing bacterial counts in vitro (**Fig. S8B**). Irrigating the wound with this non-cytotoxic concentration of hs-PAbW led to faster wound closure compared to control treatments such as water rinse and 0.9% saline, showing comparable effects to topical Neomycin application (**Figure 7E, F**). This improvement was also accompanied by a marked reduction in wound bacterial burden (**Figure 7G**).

Discussion

PAW, which contains various polyatomic ions such as NO_2^-, NO_3^-, and H_2O_2 (in this study: NO_2^- at 600 mg/L, NO_3^- at 130 mg/L, and H_2O_2 at 200 mg/L), has previously demonstrated significant potential in bacterial decontamination [46, 47]. The combination of nitric oxide and superoxide ions in acidic pH gives rise to several secondary reactive nitrogen intermediates, such as peroxynitrite ($ONOO^-$, ONOOH), which can function as nucleophilic oxidants [48, 49]. Due to its high ROS and RNS content (RONS), PAW is widely used in food and agricultural industries for disinfecting fruits and raw vegetables [11, 50]. Multiple studies showed that acidic pH stabilizes and intensifies the activity of reactive oxygen and nitrogen species [51, 52]. However, generating PAW at neutral pH is required for real world applications. In one of our previous studies, we demonstrated that using bicarbonate water can effectively buffer and maintain the

349 pH of PAW near neutrality (hs-PAbW), making it more practical for real-world applications.
350 Additionally, we showed the antimicrobial effect of hs-PAbW on *K. pneumoniae* and
351 methicillin-resistant *S. aureus* (MRSA) in the same study [21]. However, the mechanism behind
352 the bactericidal action of hs-PAbW remained unclear.

353 In this study we have seen that DCF_2DA and DAF_2DA staining of hs-PAbW, ROS-PAW, and
354 RNS-PAbW treated bacterial samples showed that the stability of RONS was equally
355 maintained in the physiological pH range (between 7 and 7.4). However, it was observed that
356 hs-PAbW is more efficient in killing exponential-phase bacteria than the stationary phase. The
357 high rate of metabolic activity and basal respiration could be a reason for the greater sensitivity
358 of the exponential phase cultures to hs-PAbW [53]. We also show that ROS-PAW, which
359 contained similar levels of ROS as hs-PAbW, couldn't kill the bacteria independently, proving
360 that their concentrations in hs-PAbW are unable to bring about the bactericidal effect
361 independently. Instead, when the bacterial strains are incubated in RNS-PAbW where RNS are
362 present at a specific proportion (as mentioned earlier), they execute the maximum bactericidal
363 activity. Incubation in ROS-PAW and RNS-PAbW resulted in changed membrane potential of
364 all the bacterial strains tested, like hs-PAbW. As reported previously, this effect may be caused
365 by lipid peroxidation mediated by reactive species present in PAW, which leads to oxidative
366 degradation of cholesterol, phospholipids, and unsaturated fatty acids, ultimately causing
367 damage to the cell membrane [54-59]. Also, previous studies had shown that the thick cell wall in
368 Gram-positive bacteria confers resistance to PAW. This can explain why we observed no
369 change in the size or stiffness of *S. aureus* upon exposure to any of the water samples [60].

370 hs-PAbW exposure generates intracellular peroxynitrite, a key reactive nitrogen species (RNS)
371 also abundant in RNS-PAbW-treated cells. Peroxynitrite induces oxidative and nitrosative
372 stress by modifying proteins, oxidizing lipids, and damaging DNA, either directly or through
373 its decomposition [61-63]. Oxidative stress induced by peroxynitrite can result from the direct

374 oxidation reactions of peroxynitrous acid or from the generation of oxidizing radicals (e.g.,
375 •OH). It leads to oxidation of thiols, heme proteins, and iron-sulfur clusters, as well as nitration
376 of tyrosine residues, which can interfere with bacterial protein function [36, 61, 64]. Due to
377 negligible peroxynitrite formation upon ROS-PAW treatment, nitrotyrosine levels were also
378 low in that condition. This shows that nitrotyrosine formation is one of the primary mechanisms
379 responsible for the bactericidal action of our hs-PAbW. We also show that RNS in hs-PAbW is
380 the key factor driving its bactericidal effect. Thus, we successfully eliminate the need for acidic
381 pH for PAW activity and have developed neutral pH hs-PAbW, enhancing its relevance for real-
382 world applications.

383 hs-PAbW effectively decontaminated non-autoclavable metal surfaces, presenting a cost-
384 effective disinfection strategy for hospital environments. A 45-minute exposure to hs-PAbW
385 resulted in significantly greater bacterial killing *in vitro* compared to high doses of antibiotics.
386 Moreover, in a murine model of *S. aureus*-infected wounds, a non-cytotoxic dose of hs-PAbW
387 promoted superior wound healing compared to 0.9% saline and comparable to topical
388 neomycin treatment. We propose a single hs-PAbW setup in hospitals, where technicians can
389 generate it via controlled electric discharges. This sustainable approach will require only
390 buffered water, minimizing raw material transport, waste, and carbon footprint. Ethically
391 sourced materials and the absence of harmful emissions will ensure safety. While hs-PAbW
392 loses efficacy after seven days, reactive species degradation can be managed with inhibitors
393 like vitamin C and isoflavones [21, 65-68]. Further research is needed to assess its environmental
394 safety post-inhibition.

395 To the best of our knowledge, this is the first study to highlight the mechanism of action of
396 neutral pH hs-PAbW and discuss its potential to prevent spread of ESKAPE pathogens.

397

Author contribution

Conceptualization: DM, ARC, LNR, and DC, Methodology: DM, PG, ARC, NV Investigation: DM, PG, ARC, NV Visualization: DM,ARC , Data curation: DM, PG, ARC, Formal analysis: DM, ARC, Fund acquisition: LNR and DC, Project administration: DM, ARC, LNR, and DC, Writing-original draft: DM, ARC, and LNR, Editing and proofreading: PG, and DC, Supervision: LNR and DC.

Acknowledgments

The authors thank the central flow cytometry facility at IISc. Mrs. Dharani and Mr. Munish from the central flow cytometry facility are acknowledged for their help in FACS data acquisition. Mrs. Deepika from Advanced Facility for Microscopy and Microanalysis (AFMM), IISc is acknowledged for her help in acquiring Scanning Electron Microscopy (SEM) images. Mrs. Monisha from Atomic Force Microscopy (AFM) Facility, Department of Bioengineering (BE), IISc, is acknowledged for her help in acquiring the AFM images.

Funding

This work was financially supported by the DAE SRC fellowship (DAE00195) and the DBT-IISc partnership umbrella program for advanced research in biological sciences and Bioengineering. Technical support from ICMR (Centre for Advanced Study in Molecular Medicine), DST (FIST), and UGC (special assistance) is duly acknowledged. DC acknowledges the ASTRA Chair professorship grant from IISc and TATA innovation fellowship grant. LNR thanks the Indian Institute of Science (IISc), Biotechnology Industry Research Assistance Council, Scheme for Transformational and Advanced Research in

Sciences (STARS), and BIRC research grant for financial support. DM thanks the IISc fellowship from MHRD, Govt. of India. PG acknowledges DBT-JRF fellowship. ARC thanks the IISc fellowship from MHRD, Govt. of India, and the late Dr. Krishna S. Kaikini estate for the Shamrao M. Kaikini and Krishna S. Kaikini scholarship. The authors thank the IISc and DST - SERB for the financial support through the research grant EMR/2017/001016.

Transparency statement

None to declare.

Data availability

All data generated for this study have been included in the manuscript.

Figures

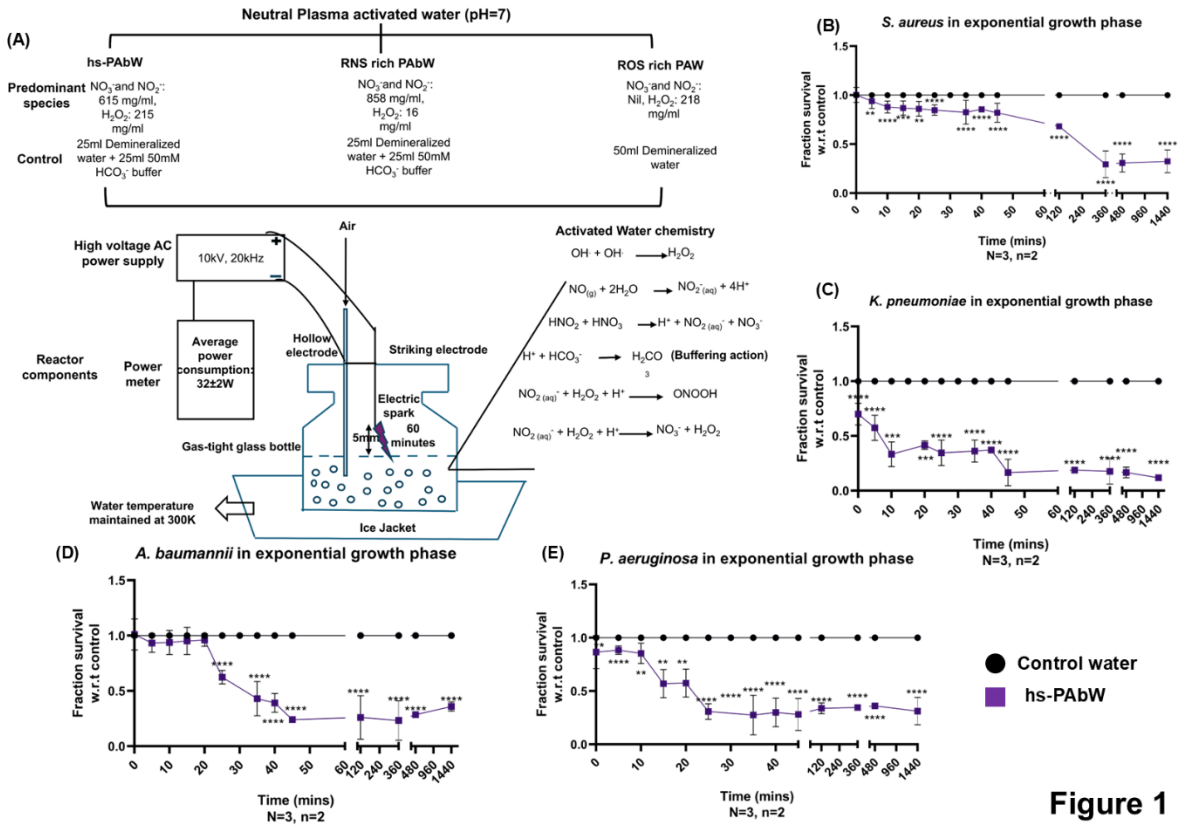

Figure 1

Figure 1. hs-PAbW induces a considerable amount of killing in exponentially growing bacteria.

(A) Schematic depicting the generation of hs-PAbW, RNS-PAbW, and ROS-PAW. Line graphs illustrate fraction survival relative to the control treatment over exposure times ranging from 0 to 1440 minutes for *S. aureus* (B), *K. pneumoniae* (C), *A. baumannii* (D), and *P. aeruginosa* (E). The data are represented as mean ± SD of data points from 3 independent experiments. (N=3, n=2,).

(P)* *< 0.05, *(P)* **< 0.005, *(P)* ***< 0.0005, *(P)* *< 0.0001, ns= non-significant, (Unpaired two-tailed student's t-test).**

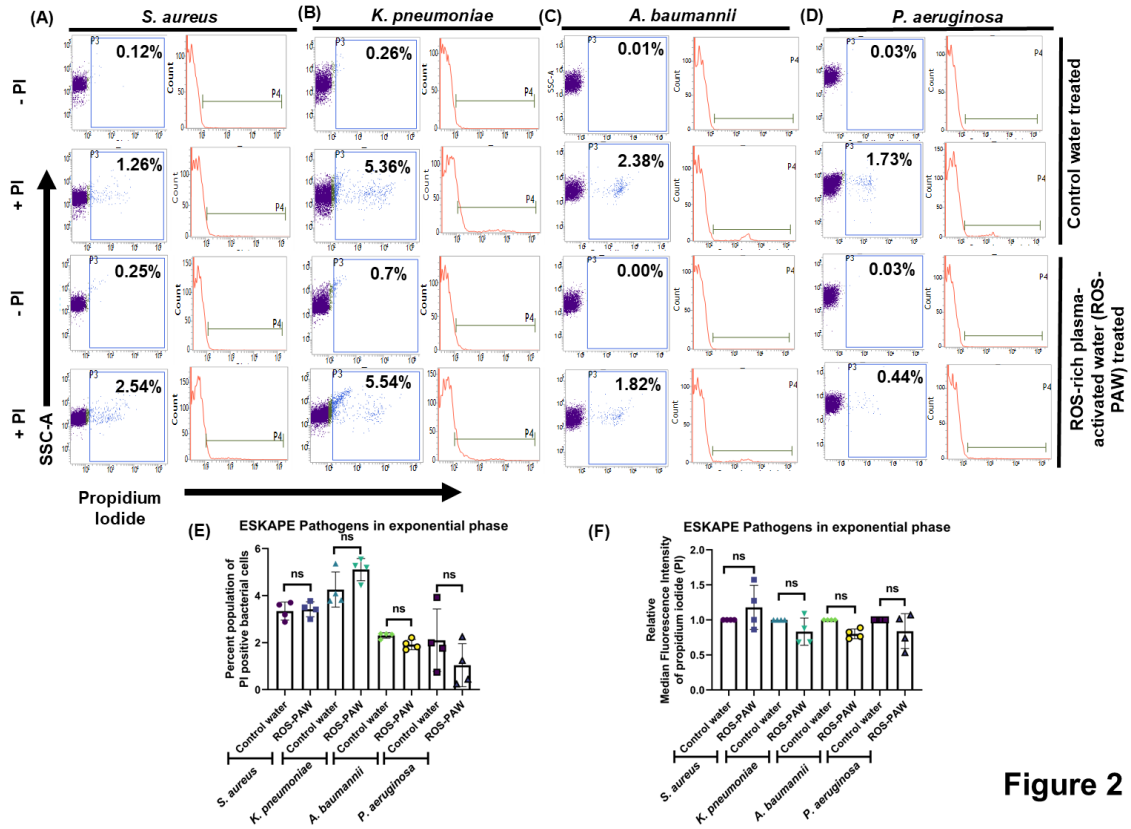

Figure 2. ROS-PAW itself is unable to induce bacterial death.

(A, B, C, and D) The dot plot (SSC-A vs. PI) and histogram (count vs. PI) represent the viability of exponentially growing *S. aureus* (A), *K. pneumoniae* (B), *A. baumannii* (C), and *P. aeruginosa* (D) treated with reactive oxygen species rich plasma-activated water (ROS-PAW). (D) The bar graphs represent the PI-positive percent population of *S. aureus*, *K. pneumoniae*, *A. baumannii*, and *P. aeruginosa* with or without ROS-PAW treatment. (E) The median

fluorescence intensity (MFI) of the PI-positive population of *S. aureus*, *K. pneumoniae*, *A. baumannii*, and *P. aeruginosa* with or without ROS-PAW treatment (F). The data are representative of n≥3, N=3 and are presented as mean ± SD

(P)* *< 0.05, *(P)* **< 0.005, *(P)* ***< 0.0005, *(P)* *< 0.0001, ns= non-significant, (Unpaired two-tailed student's t-test).**

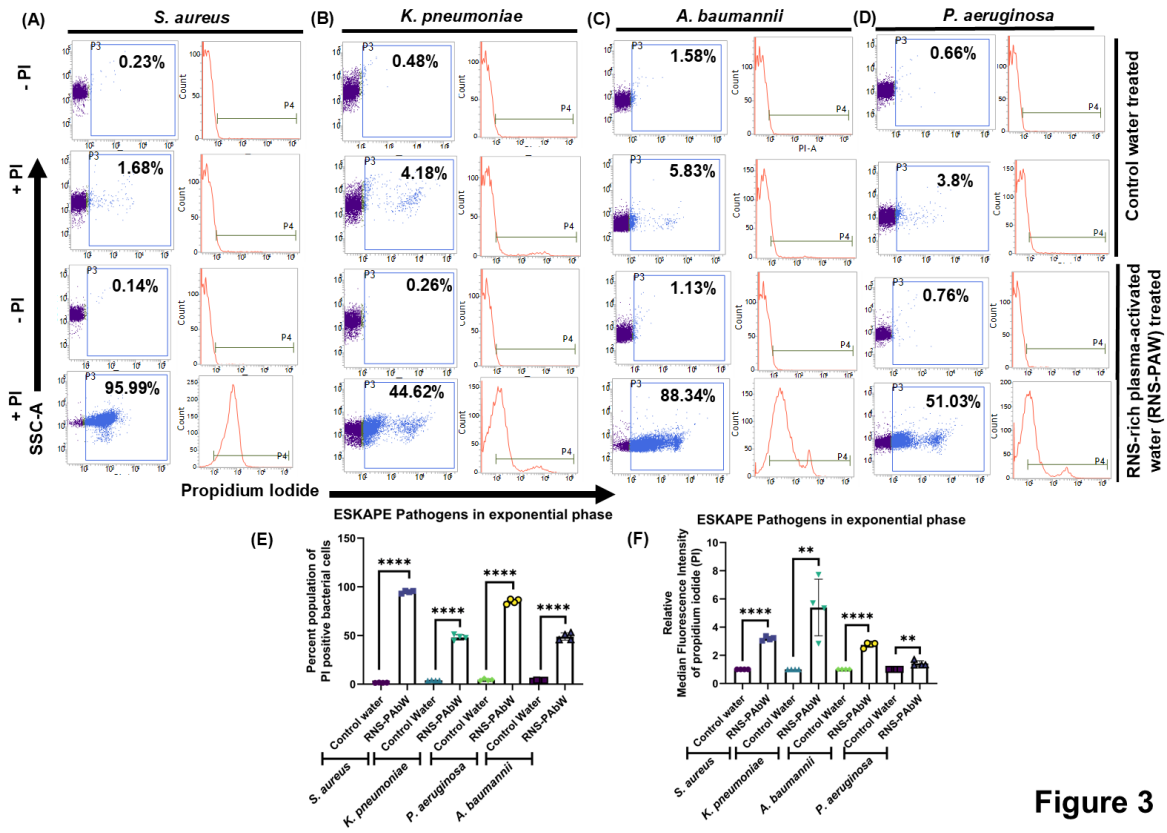

Figure 3. RNS-PAbW can independently kill exponentially growing bacteria.

(A, B, C, and D) The dot plot (SSC-A vs. PI) and histogram (count vs. PI) represent the viability of exponentially growing *S. aureus* (A), *K. pneumoniae* (B), *A. baumannii* (C), and *P. aeruginosa* (D) treated with reactive nitrogen species rich plasma-activated water (RNS-PAbW). The bar graphs represent the PI-positive percent population of *S. aureus*, *K. pneumoniae*, *A. baumannii*, and *P. aeruginosa* with or without RNS-PAbW treatment. (E) The relative median fluorescence intensity (MFI) of the PI-positive population of *S. aureus*, *K. pneumoniae*, *A. baumannii*, and *P. aeruginosa* with or without RNS-PAbW treatment (F). The data are representative of n≥3, N=3 and are presented as mean ± SD

(P)* *< 0.05, *(P)* **< 0.005, *(P)* ***< 0.0005, *(P)* *< 0.0001, ns= non-significant, (Unpaired two-tailed student's t-test).**

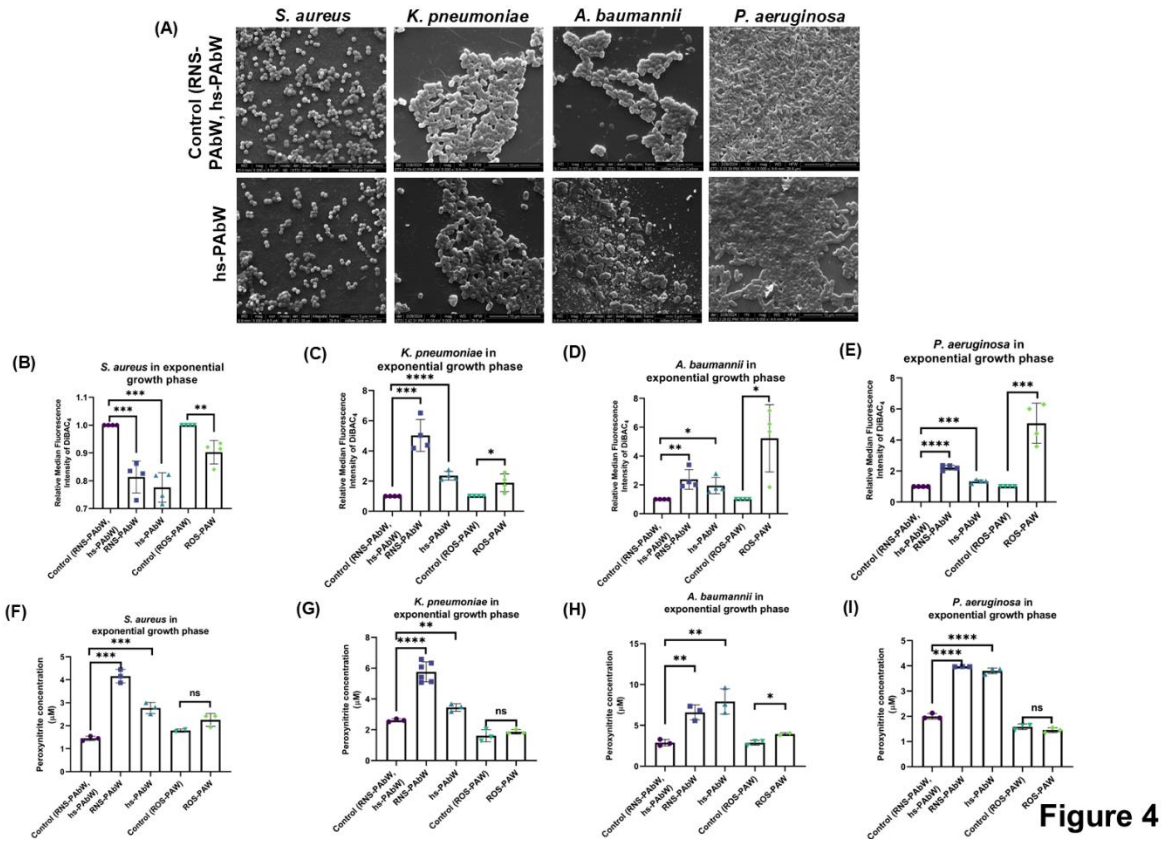

Figure 4. ROS-PAW can alter membrane potential, however, it is not sufficient for a bactericidal effect.

Scanning Electron Microscopy images of *S. aureus*, *K. pneumoniae*, *A. baumannii*, *P. aeruginosa* treated with hs-PAbW and control water (5000X magnification) (A). The relative median fluorescence intensity (MFI) of the $DiBAC_4$-positive population of *S. aureus*, *K. pneumoniae*, *A. baumannii*, and *P. aeruginosa* with RNS-PAbW, hs-PAbW, ROS-PAW treatment. is represented in figure panels B-E. The data are representative of n≥3, N=3 and are presented as mean ± SD. Figure panels **F-I** contain the bar graphs that represent the quantity of intracellular peroxynitrite produced upon treatment with control ROS-PAW, ROS-PAW, control RNS-PAbW, RNS-PAbW, control hs-PAbW and hs-PAbW of *S. aureus* (B), *K. pneumoniae* (C), *A. baumannii* (D), *P. aeruginosa* (E). The data are representative of n≥3, N=3 and are presented as mean ± SD

482 ***(P)* *< 0.05, *(P)* **< 0.005, *(P)* ***< 0.0005, *(P)* ****< 0.0001, ns= non-significant,**
483 **(Unpaired two-tailed student's t-test).**

484

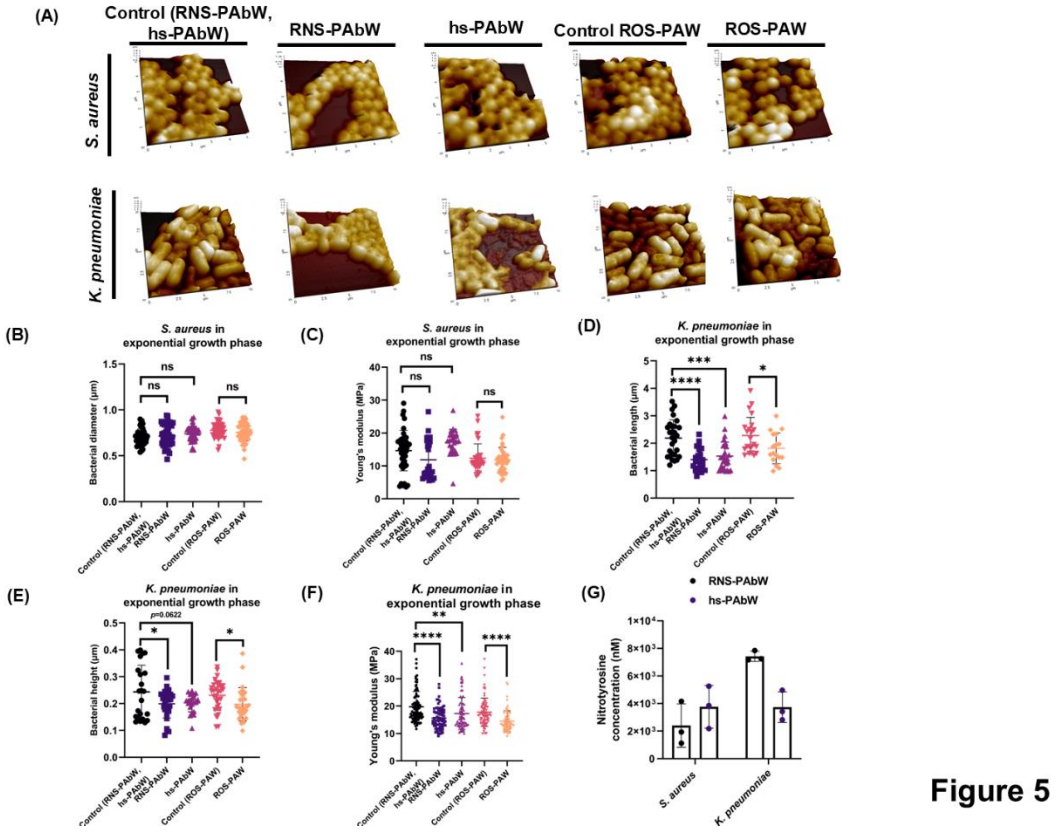

486 **Figure 5. Treatment with RNS-PAbW, hs-PAbW, and ROS-PAbW caused a reduction in**
487 **the length, height, and Young's modulus of the Gram-negative bacterium *K. pneumoniae***
488 **although ROS-PAW was unrelated to increased nitrotyrosine levels in *S. aureus* and *K.***
489 ***pneumoniae***

490 (A) Atomic Force Microscopy images of *S. aureus* and *K. pneumoniae* after treatment with
491 control waters, ROS-PAW, hs-PAbW, and RNS-PAbW. Quantification of the length, height,
492 and Young's modulus for *S. aureus* (B, C, D) and *K. pneumoniae* (E, F, G) was performed. Data
493 for (A-G) are representative data of N=2, n≥20, and are shown as mean±SD. (H) shows
494 intracellular nitrotyrosine levels in *S. aureus* and *K. pneumoniae* following treatment with
495 RNS-PAbW and hs-PAbW. The data is a representative of N=2, n=3, and is presented as
496 mean±SD.

(P)* *< 0.05, *(P)* **< 0.005, *(P)* ***< 0.0005, *(P)* *< 0.0001, ns= non-significant, (Unpaired two-tailed student's t-test).**

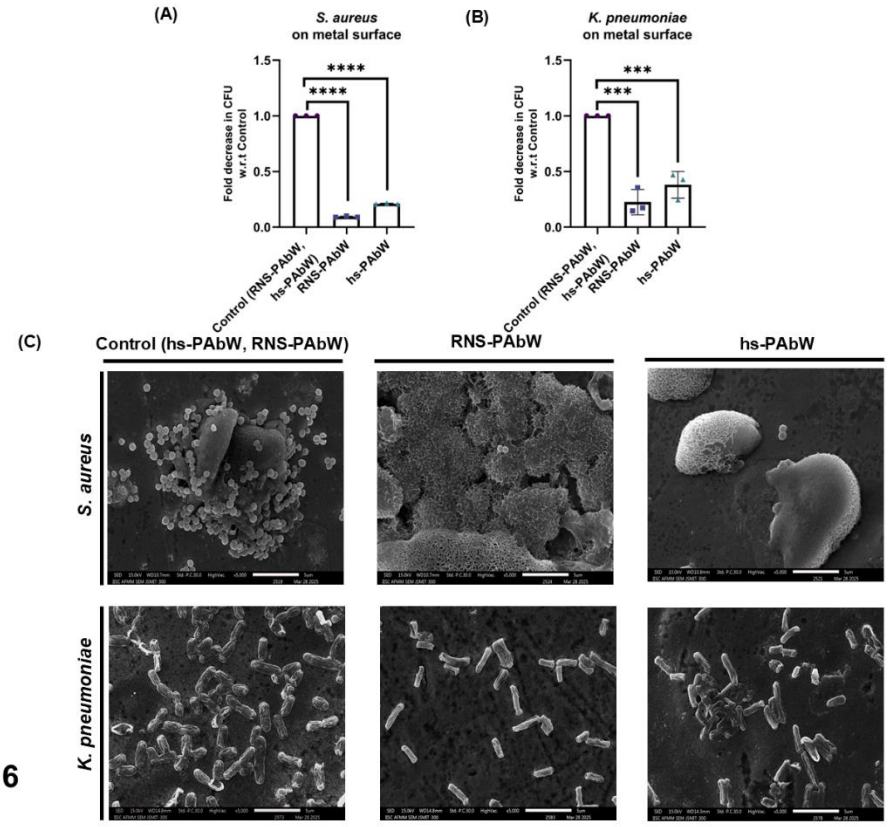

Figure 6

Figure 6. hs-PAbW can successfully reduce bacterial burden on non-autoclavable metal surfaces

Bar graphs (A) and (B) depict the fold reduction in CFU after treatment with hs-PAbW and RNS-PAbW on *S. aureus* (A) and *K. pneumoniae* (B) droplets dried on metal surfaces. The data are represented as mean ± SEM. (N=3, n=2). Figure panel (G) includes SEM images of *S. aureus* and *K. pneumoniae* on stainless steel surface after cleansing with control water, hs-PAbW, RNS-PAbW (5000X magnification).

(P)* *< 0.05, *(P)* **< 0.005, *(P)* ***< 0.0005, *(P)* *< 0.0001, ns= non-significant, (Unpaired two-tailed student's t-test).**

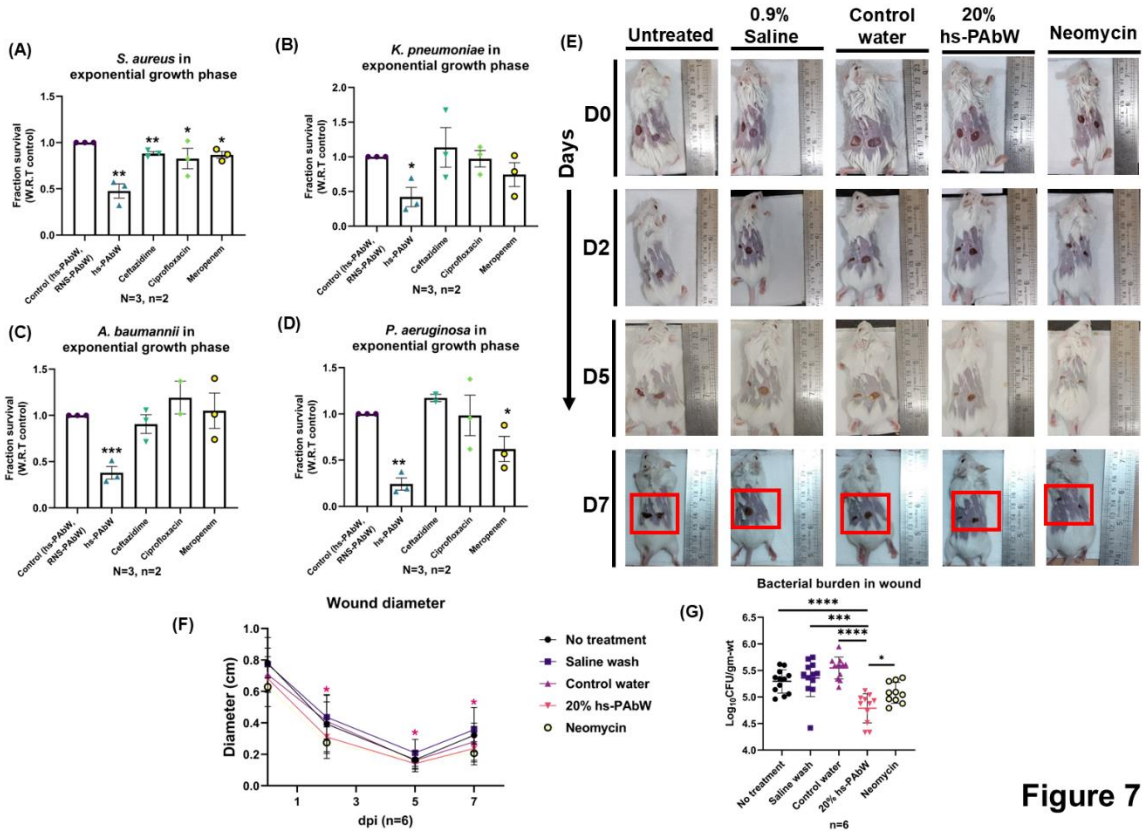

Figure 7: hs-PAbW was more effective at killing ESKAPE pathogens than high doses of antibiotics, and a non-cytotoxic dose of the same can be used as a wound irrigation agent

Bar graphs (A-D) depict the reduction in CFU of *S. aureus*, *K. pneumoniae*, *A. baumannii*, *P. aeruginosa* after treatment with hs-PAbW and 50 µg/ml of ceftazidime, meropenem, and ciprofloxacin *in-vitro*. The data are represented as mean ± SEM. (N=3, n=2). The images show wound closure in Balb/c mice infected with *S. aureus*, following treatment with various irrigation methods including 0.9% saline, control water, hs-PAbW, and neomycin. Wound diameter (F) and bacterial load (G) were quantified, with data presented as mean ± SD for n = 6.

(P)* *< 0.05, *(P)* **< 0.005, *(P)* ***< 0.0005, *(P)* *< 0.0001, ns= non-significant, (Unpaired two-tailed student's t-test) (Mann-Whitney U-test for *in-vivo* experiments).**

Supplementary Figures

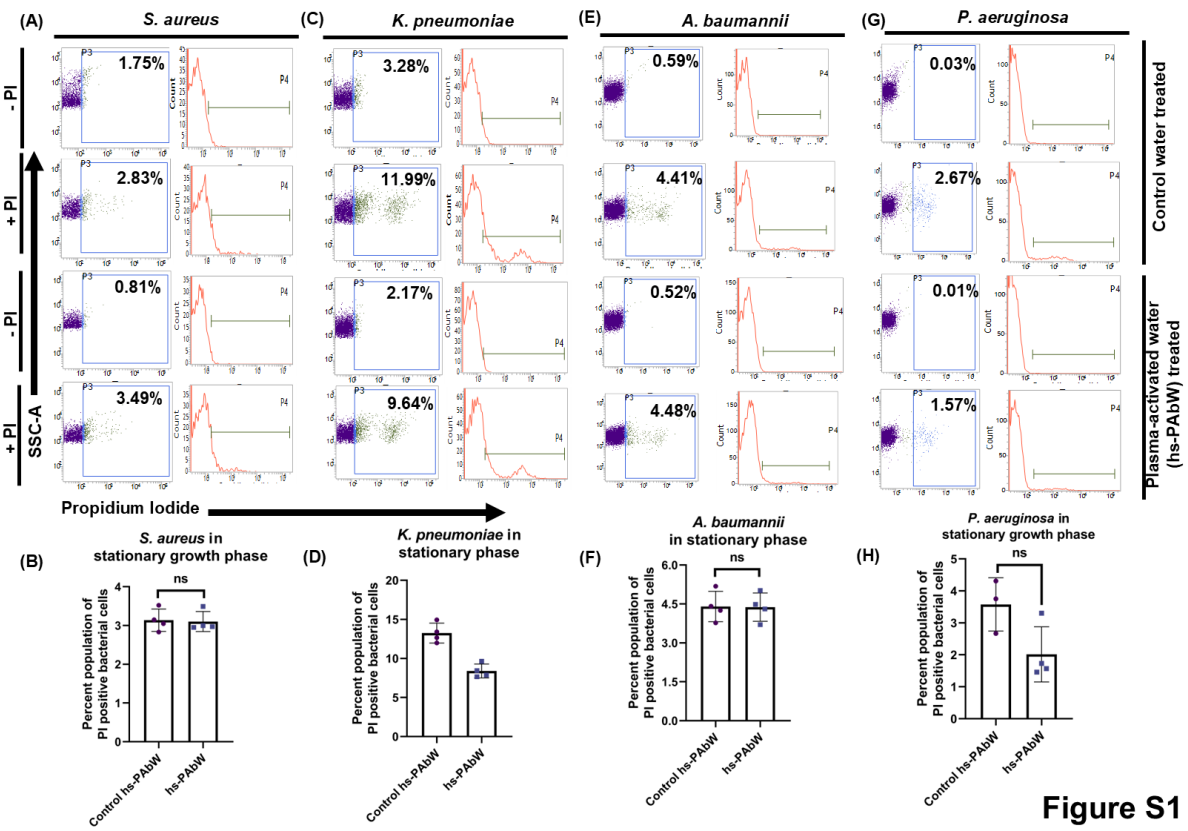

Figure S1. hs-PAbW couldn't kill the stationary phase cultures of bacteria.

(A, C, E and G) The dot plot (SSC-A vs. PI) and histogram (count vs. PI) represent the viability of exponentially growing cultures of *S. aureus* (A), *K. pneumoniae* (C), *A. baumannii* (E), and *P. aeruginosa* (E) with hs-PAbW. The bar graphs represent the propidium iodide positive percent population of *S. aureus* (B), *K. pneumoniae* (D), *A. baumannii* (F), and *P. aeruginosa* (H) with or without hs-PAbW treatment. The data are representative of n≥3, N=3 and is presented as mean ± SD.

(P)* *< 0.05, *(P)* **< 0.005, *(P)* ***< 0.0005, *(P)* *< 0.0001, ns= non-significant, (Unpaired two-tailed student's t-test).**

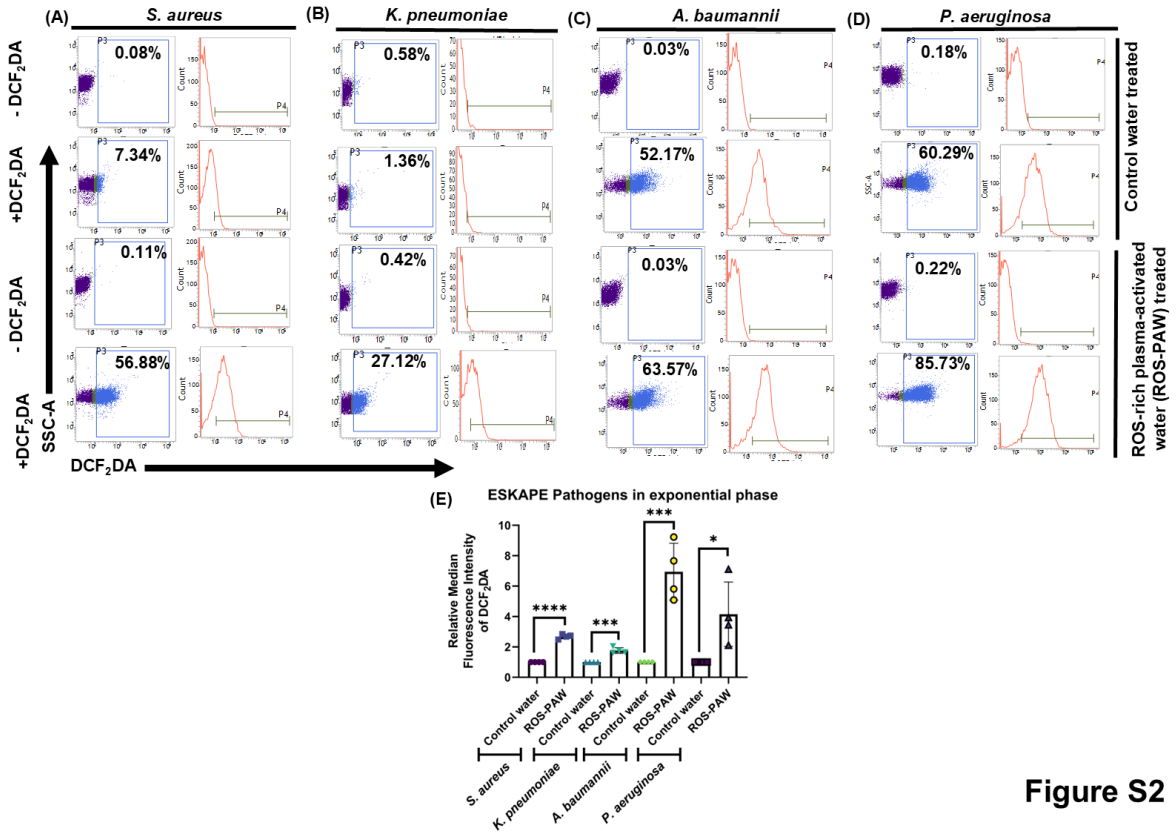

Figure S2

Figure S2. ROS-PAW generates a significant amount of ROS.

(A, B, C, and D) The dot plot (SSC-A vs. DCF_2DA) and histogram (count vs. DCF_2DA) represent the ROS content of exponentially growing *S. aureus* (A), *K. pneumoniae* (B), *A. baumannii* (C), and *P. aeruginosa* (D) treated with reactive oxygen species rich plasma-activated water (ROS-PAW). The bar graphs represent the relative median fluorescence intensity (MFI) of the DCF_2DA-positive population of *S. aureus*, *K. pneumoniae*, *A. baumannii*, and *P. aeruginosa* with or without ROS-PAW treatment (E). The data are representative of n≥3, N=3 and is presented as mean ± SD.

(P)* *< 0.05, *(P)* **< 0.005, *(P)* ***< 0.0005, *(P)* *< 0.0001, ns= non-significant, (Unpaired two-tailed student's t-test).**

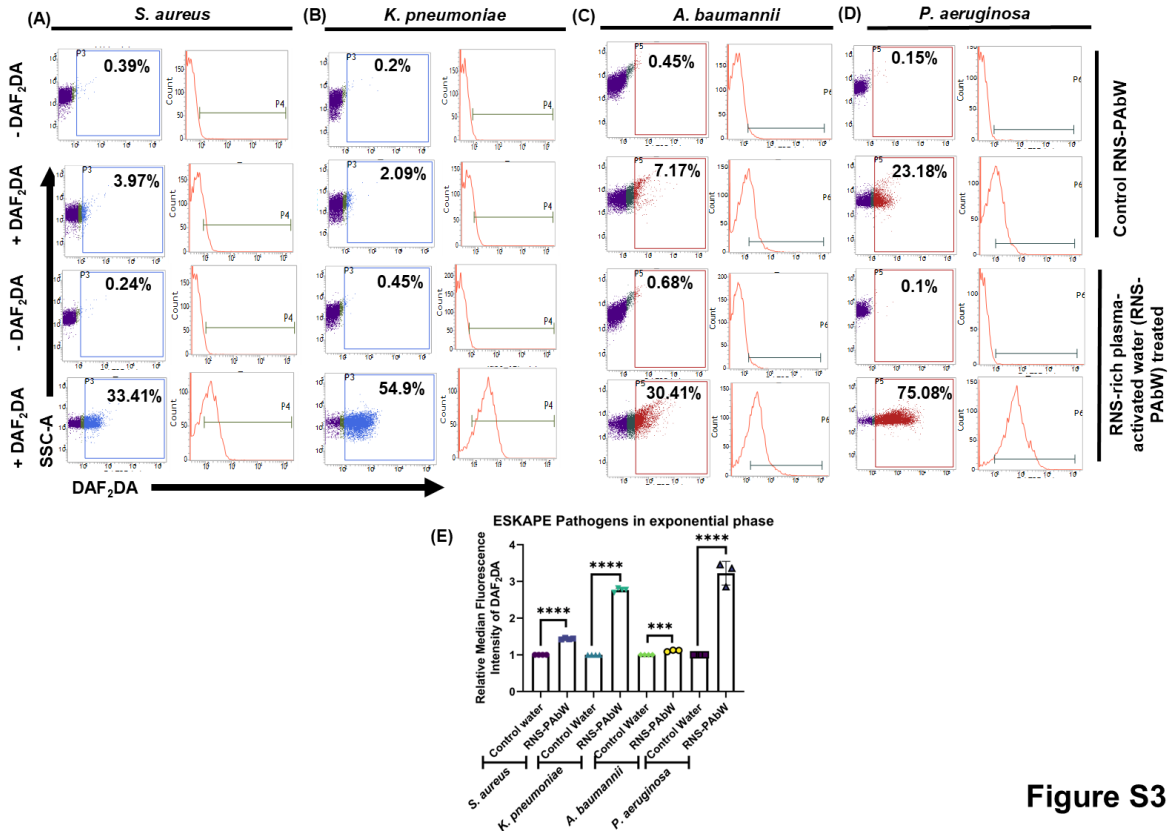

Figure S3

Figure S3. RNS-PAbW generates high amount of reactive nitrogen species in the treated bacteria.

(A, B, C, and D) The dot plot (SSC-A vs. DAF_2DA) and histogram (count vs. DAF_2DA) represent the RNS content of exponentially growing *S. aureus* (A), *K. pneumoniae* (B), *A. baumannii* (C), and *P. aeruginosa* (D) treated with reactive nitrogen species rich plasma-activated water (RNS-PAbW). The bar graphs represent the median fluorescence intensity (MFI) of the DAF_2DA-positive population of *S. aureus*, *K. pneumoniae*, *A. baumannii*, and *P. aeruginosa* with or without RNS-PAbW treatment (E). The data are representative of n≥3, N=3 and is presented as mean ± SD.

(P)* *< 0.05, *(P)* **< 0.005, *(P)* ***< 0.0005, *(P)* *< 0.0001, ns= non-significant, (Unpaired two-tailed student's t-test).**

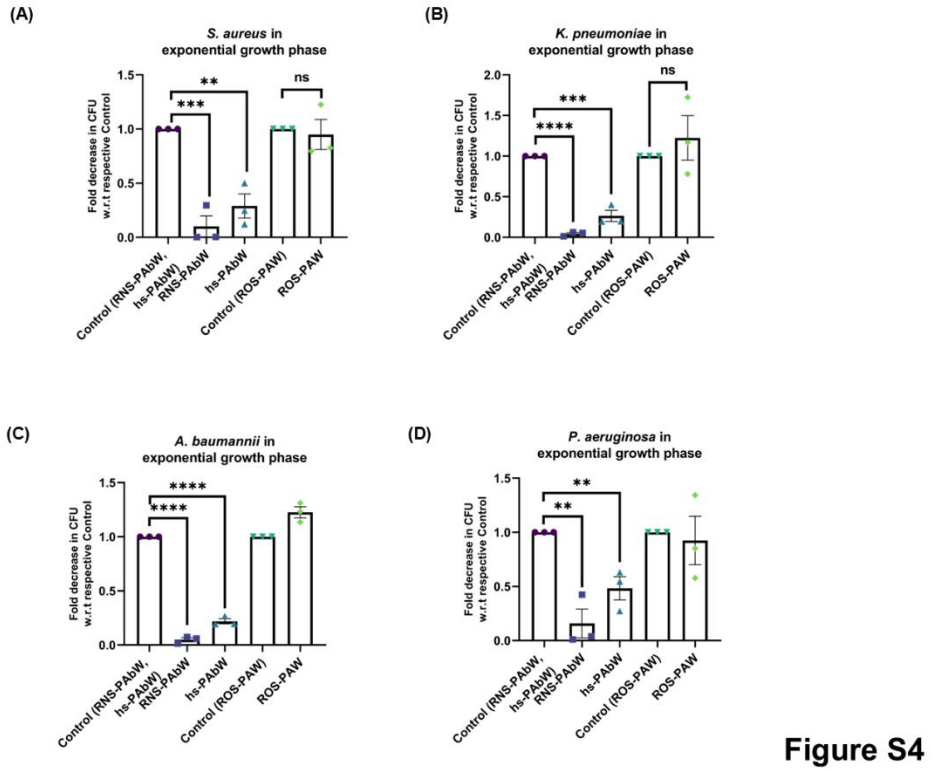

Figure S4. Incubation with RNS-PAbW and hs-PAbW results in significant reduction of Colony Forming Units, but not ROS-PAW

The column graphs represent the fold decrease in CFU after treatment with RNS-PAbW, hs-PAbW, and ROS-PAW compared to the respective control water samples for *S. aureus* (A), *K. pneumoniae* (B), *A. baumannii* (C), and *P. aeruginosa* (D). The data are represented as mean ± SEM. (n=2, N=3).

(P)* *< 0.05, *(P)* **< 0.005, *(P)* ***< 0.0005, *(P)* *< 0.0001, ns= non-significant, (Unpaired two-tailed student's t-test).**

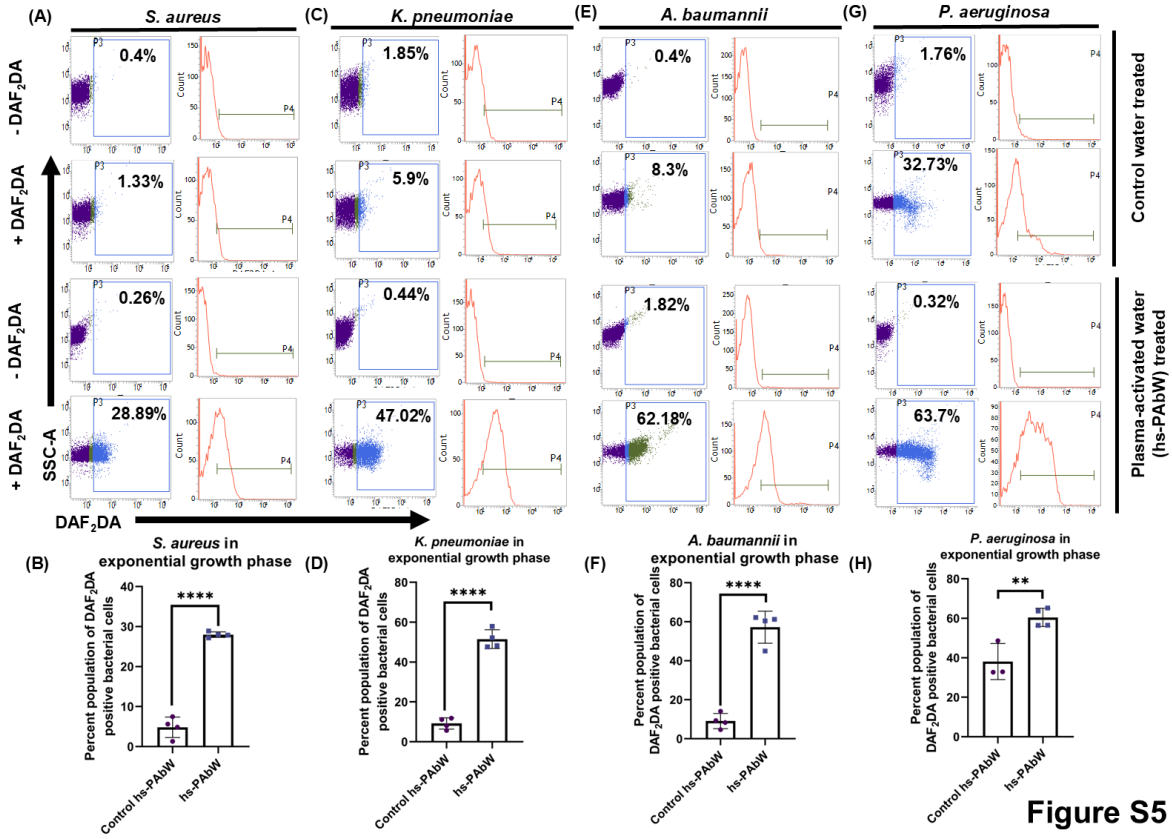

Figure S5. hs-PAbW-dependent generation of reactive nitrogen species while incubated with exponential-phase bacteria.

(A, C, E and G) The dot plot (SSC-A vs. DAF_2DA) and histogram (count vs. DAF_2DA) represent the generation of reactive nitrogen intermediates upon treating the exponentially growing cultures of *S. aureus* (A), *K. pneumoniae* (C), *A. baumannii* (E), and *P. aeruginosa* (E) with hs-PAbW. The bar graphs represent the DAF_2DA-positive percent population of *S. aureus* (B), *K. pneumoniae* (D), *A. baumannii* (F), and *P. aeruginosa* (H) with or without hs-PAbW treatment. The data are representative of n≥3, N=3 and is presented as mean ± SD.

(P)* *< 0.05, *(P)* **< 0.005, *(P)* ***< 0.0005, *(P)* *< 0.0001, ns= non-significant, (Unpaired two-tailed student's t-test).**

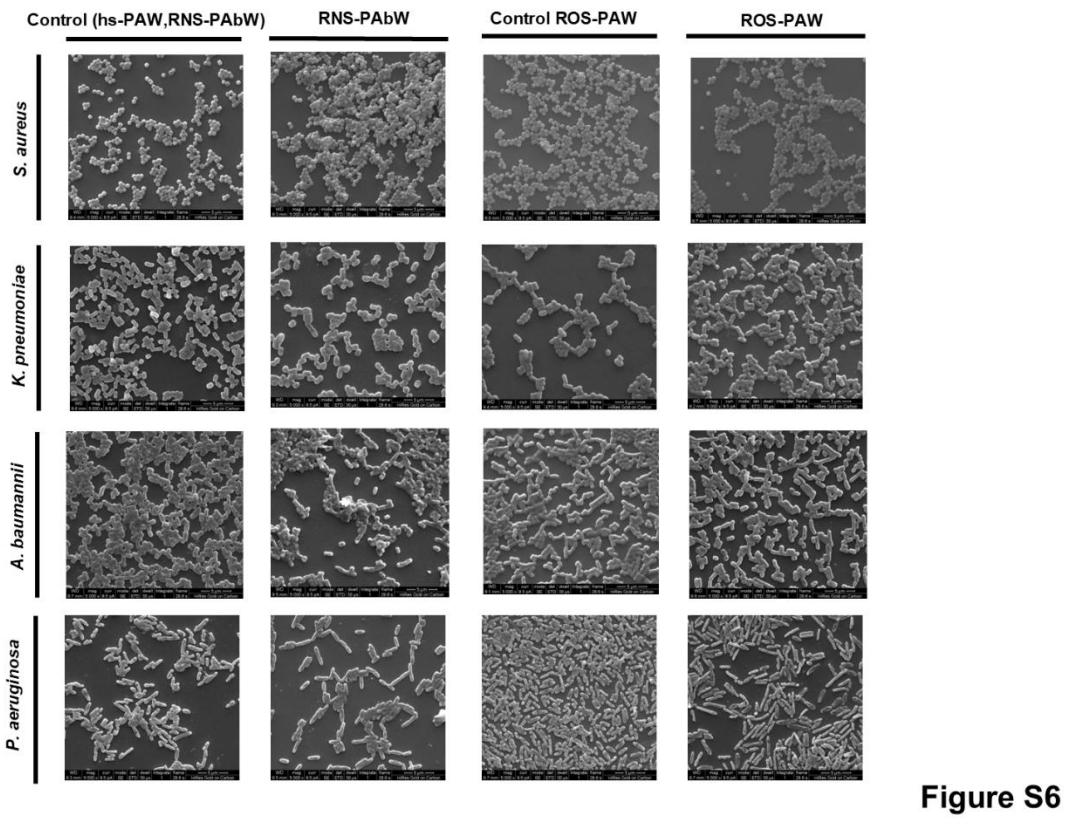

583

584 **Figure S6. Scanning Electron Microscopy to study morphological change in the bacterial**

585 **samples post exposure to RNS-PAbW and ROS-PAW** (5000X magnification)

586

(A)

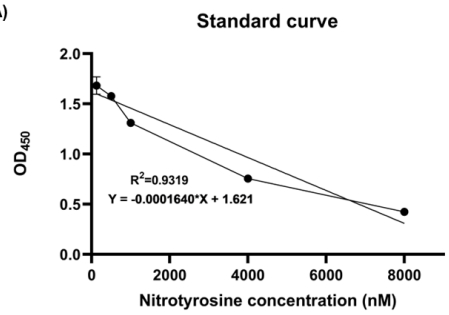

(B)

OD_{450}	OD_{450}	OD_{450}		
2.2022	2.1626	2.088	Control (RNS-PAbW, PAbW)	*S. aureus*
1.0671	1.5135	1.3933	RNS-PAbW	
0.906	1.3581	1.1124	hs-PAbW	
3.5378	3.344	3.6628	Control ROS-PAW	
3.696	3.4822	3.6582	ROS-PAW	
2.059	2.0361	1.7912	Control (RNS-PAbW, PAbW)	*K. pneumoniae*
0.6262	0.5272	0.615	RNS-PAbW	
0.9492	1.2645	1.1758	hs-PAbW	
3.0252	3.0718	2.9592	Control ROS-PAW	
3.0177	3.0131	3.236	ROS-PAW	

Figure S7

Figure S7: Nitrotyrosine estimation reveals a significant increase in nitrotyrosine levels following treatment with RNS-PAbW and hs-PAbW, but not with ROS-PAW.

A standard curve (A) was generated using the OD_{450} absorbance values of the nitrotyrosine standards, and the nitrotyrosine concentration in the samples was determined by interpolating the raw data (B) against the standard curve.

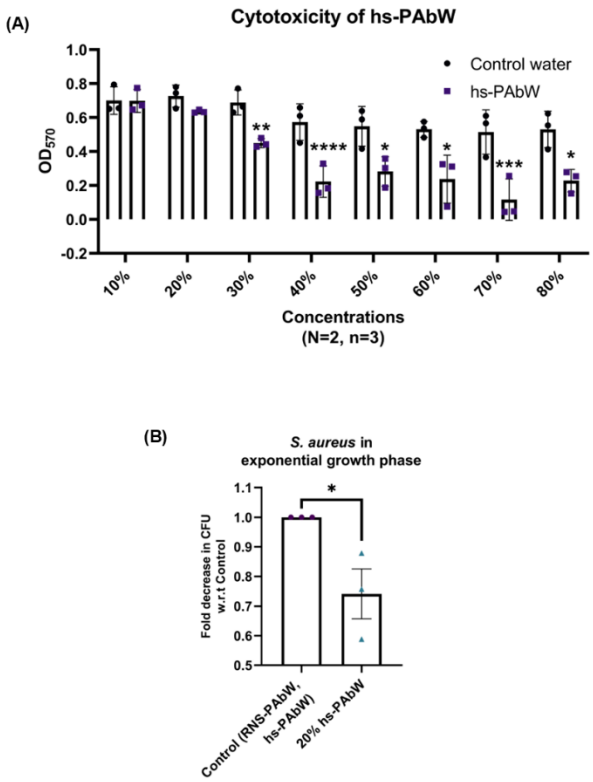

Figure S8

Figure S8: A non-cytotoxic dose of hs-PAbW was also able to retain its bactericidal effect

Figure showing MTT Assay of different concentrations of hs-PAbW (A) and the fold reduction in CFU after treatment with non-cytotoxic dose of hs-PAbW (B). (A) is representative of N=2, n=3 and is expressed as mean± SD and (B) is merged data of N=3, n=2, and is expressed as mean± SEM.

(P)* *< 0.05, *(P)* **< 0.005, *(P)* ***< 0.0005, *(P)* *< 0.0001, ns= non-significant, (One-way ANOVA with mixed effect-analysis for grouped data) (Unpaired two-tailed student's t-test for column graph).**

Reference

1. Prestinaci F, Pezzotti P, Pantosti A. Antimicrobial resistance: a global multifaceted phenomenon. *Pathog Glob Health* 2015; **109**: 309-18.
2. Larsson DGJ, Flach CF. Antibiotic resistance in the environment. *Nat Rev Microbiol* 2022; **20**: 257-69.
3. Antimicrobial Resistance C. Global burden of bacterial antimicrobial resistance in 2019: a systematic analysis. *Lancet* 2022; **399**: 629-55.
4. Roy Chowdhury A, Hajra D, Mukherjee D et al. Functional OmpA of Salmonella Typhimurium provides protection from lysosomal degradation and inhibits autophagic processes in macrophages. *J Infect Dis* 2024.

5. Rajan A, Boopathy B, Radhakrishnan M et al. Plasma processing: a sustainable technology in agri-food processing. *Sustainable Food Technology* 2023; **1**: 9-49.
6. Thirumdas R, Kothakota A, Annapure U et al. Plasma activated water (PAW): Chemistry, physico-chemical properties, applications in food and agriculture. *Trends in Food Science & Technology* 2018; **77**: 21-31.
7. Girard PM, Arbabian A, Fleury M et al. Synergistic Effect of H2O2 and NO2 in Cell Death Induced by Cold Atmospheric He Plasma. *Sci Rep* 2016; **6**: 29098.
8. Hoeben WFLM, van Ooij PP, Schram DC et al. On the Possibilities of Straightforward Characterization of Plasma Activated Water. *Plasma Chemistry and Plasma Processing* 2019; **39**: 597-626.
9. Punith N, Harsha R, Lakshminarayana R et al. Plasma Activated Water Generation and its Application in Agriculture. *Advanced Materials Letters* 2019; **10**: 700-4.
10. Rathore V, Nema SK. Optimization of process parameters to generate plasma activated water and study of physicochemical properties of plasma activated solutions at optimum condition. *Journal of Applied Physics* 2021; **129**.
11. Soni A, Choi J, Brightwell G. Plasma-Activated Water (PAW) as a Disinfection Technology for Bacterial Inactivation with a Focus on Fruit and Vegetables. *Foods* 2021; **10**.
12. Li Y, Pan J, Ye G et al. In vitro studies of the antimicrobial effect of non-thermal plasma-activated water as a novel mouthwash. *Eur J Oral Sci* 2017; **125**: 463-70.
13. Guo L, Yao Z, Yang L et al. Plasma-activated water: An alternative disinfectant for S protein inactivation to prevent SARS-CoV-2 infection. *Chem Eng J* 2021; **421**: 127742.
14. Zhao YM, Patange A, Sun DW et al. Plasma-activated water: Physicochemical properties, microbial inactivation mechanisms, factors influencing antimicrobial effectiveness, and applications in the food industry. *Compr Rev Food Sci Food Saf* 2020; **19**: 3951-79.
15. Rifna EJ, Ratish Ramanan K, Mahendran R. Emerging technology applications for improving seed germination. *Trends in Food Science & Technology* 2019; **86**: 95-108.
16. Li Y, Sun K, Ye G et al. Evaluation of Cold Plasma Treatment and Safety in Disinfecting 3-week Root Canal Enterococcus faecalis Biofilm In Vitro. *J Endod* 2015; **41**: 1325-30.
17. Kim S, Kim CH. Applications of Plasma-Activated Liquid in the Medical Field. *Biomedicines* 2021; **9**.
18. Ali M, Cheng JH, Sun DW. Effect of plasma activated water and buffer solution on fungicide degradation from tomato (Solanum lycopersicum) fruit. *Food Chem* 2021; **350**: 129195.
19. Lukes P, Dolezalova E, Sisrova I et al. Aqueous-phase chemistry and bactericidal effects from an air discharge plasma in contact with water: evidence for the formation of peroxynitrite through a pseudo-second-order post-discharge reaction of H2O2and HNO2. *Plasma Sources Science and Technology* 2014; **23**: 015019.
20. Mwakalesi AJ, Nyangi M. Effective Corrosion Inhibition of Mild Steel in an Acidic Environment Using an Aqueous Extract of Macadamia Nut Green Peel Biowaste. *Engineering Proceedings* 2023; **31**: 41.
21. Boopathy B, Mukherjee D, Nishanth V et al. Generation of Species-Specific High-Strength Plasma Activated Water at Neutral pH and its Antimicrobial Characteristics. *Plasma Chemistry and Plasma Processing* 2024; **44**: 1003-17.
22. N. P, Singh AK, J. A et al. Generation of neutral pH high-strength plasma-activated water from a pin to water discharge and its bactericidal activity on multidrug-resistant pathogens. *Plasma Processes and Polymers* 2023; **20**: 2200133.
23. Morris FC, Dexter C, Kostoulias X et al. The Mechanisms of Disease Caused by Acinetobacter baumannii. *Front Microbiol* 2019; **10**: 1601.
24. Qin S, Xiao W, Zhou C et al. Pseudomonas aeruginosa: pathogenesis, virulence factors, antibiotic resistance, interaction with host, technology advances and emerging therapeutics. *Signal Transduct Target Ther* 2022; **7**: 199.

664 25. Ramakrishnan R, Nair AV, Parmar K et al. Combating biofilm-associated Klebsiella pneumoniae
665 infections using a bovine microbial enzyme. *NPJ Biofilms Microbiomes* 2024; **10**: 119.
666 26. Zhou X, He P. Improved measurements of intracellular nitric oxide in intact microvessels using
667 4,5-diaminofluorescein diacetate. *Am J Physiol Heart Circ Physiol* 2011; **301**: H108-14.
668 27. Walch M, Dotiwala F, Mulik S et al. Cytotoxic cells kill intracellular bacteria through granulysin-
669 mediated delivery of granzymes. *Cell* 2014; **157**: 1309-23.
670 28. Chowdhury AR, Mukherjee D, Singh AK et al. Loss of outer membrane protein A (OmpA)
671 impairs the survival of Salmonella Typhimurium by inducing membrane damage in the presence of
672 ceftazidime and meropenem. *J Antimicrob Chemother* 2022; **77**: 3376-89.
673 29. Yang Y, Xie W, Li S et al. Splint-free line drawing model: An innovative method for excisional
674 wound models. *Int Wound J* 2023; **20**: 2673-8.
675 30. Powell D, Comer B, Wu B et al. Effect of Commercially Available Wound Irrigation Solutions on
676 Uninfected Host Tissue in a Murine Model. *Arthroplast Today* 2024; **25**: 101300.
677 31. Ghoshal A, Shah A, Balaji KN. Deregulation of epigenetic factor, KDM6A, is involved during
678 Candida albicans mediated delayed wound healing. *bioRxiv* 2024: 2024.12.09.627481.
679 32. Ju S, Li B, Yang X et al. Plasma-activated water for inactivation of Fusarium graminearum
680 spores: An in-vitro wheat study. *LWT* 2023; **183**: 114815.
681 33. Goldstein S, Merenyi G. The chemistry of peroxynitrite: implications for biological activity.
682 *Methods Enzymol* 2008; **436**: 49-61.
683 34. Ischiropoulos H. Biological tyrosine nitration: a pathophysiological function of nitric oxide and
684 reactive oxygen species. *Arch Biochem Biophys* 1998; **356**: 1-11.
685 35. Liaudet L, Soriano FG, Szabo C. Biology of nitric oxide signaling. *Crit Care Med* 2000; **28**: N37-
686 52.
687 36. Gunaydin H, Houk KN. Mechanisms of peroxynitrite-mediated nitration of tyrosine. *Chem Res*
688 *Toxicol* 2009; **22**: 894-8.
689 37. Prolo C, Alvarez MN, Radi R. Peroxynitrite, a potent macrophage-derived oxidizing cytotoxin to
690 combat invading pathogens. *BioFactors* 2014; **40**: 215-25.
691 38. Pochtovyi AA, Vasina DV, Kustova DD et al. Contamination of Hospital Surfaces with Bacterial
692 Pathogens under the Current COVID-19 Outbreak. *Int J Env Res Public Health* 2021; **18**: 9042.
693 39. Otokunefor K, Famakin BO, Douglas DO. Assessment of door handles as potential reservoirs of
694 drug-resistant enterococci. *Bulletin of the National Research Centre* 2020; **44**: 203.
695 40. Ko WC, Stone GG. In vitro activity of ceftazidime-avibactam and comparators against Gram-
696 negative bacterial isolates collected in the Asia-Pacific region as part of the INFORM program (2015-
697 2017). *Ann Clin Microbiol Antimicrob* 2020; **19**: 14.
698 41. Bulik CC, Fauntleroy KA, Jenkins SG et al. Comparison of meropenem MICs and susceptibilities
699 for carbapenemase-producing Klebsiella pneumoniae isolates by various testing methods. *J Clin*
700 *Microbiol* 2010; **48**: 2402-6.
701 42. Sheng WH, Lin YC, Wang JT et al. Identification of distinct ciprofloxacin susceptibility in
702 Acinetobacter spp. by detection of the gyrA gene mutation using real-time PCR. *Mol Cell Probes* 2009;
703 **23**: 154-6.
704 43. Chang MX, Zhang JF, Sun YH et al. Contribution of Different Mechanisms to Ciprofloxacin
705 Resistance in Salmonella spp. *Front Microbiol* 2021; **12**: 663731.
706 44. Chaudhuri D, Roy Chowdhury A, Biswas B et al. Salmonella Typhimurium Infection Leads to
707 Colonization of the Mouse Brain and Is Not Completely Cured With Antibiotics. *Front Microbiol* 2018;
708 **9**: 1632.
709 45. Ramakrishnan R, Nair AV, Parmar K et al. Combating biofilm-associated Klebsiella pneumoniae
710 infections using a bovine microbial enzyme. *npj Biofilms and Microbiomes* 2024; **10**: 119.
711 46. Perinban S, Orsat V, Lyew D et al. Effect of plasma activated water on Escherichia coli
712 disinfection and quality of kale and spinach. *Food Chem* 2022; **397**: 133793.

47. Droste NC, Hummert M, Leenders P et al. Plasma-Activated Tap Water with Oxidative Potential Has an Inactivating Effect on Microbiological Contaminants in Aqueous Suspensions. *Pathogens* 2024; **13**.
48. Mizoi K, Rodriguez-Gonzalez V, Sasaki M et al. Interactions between pH, reactive species, and cells in plasma-activated water can remove algae. *RSC Adv* 2022; **12**: 7626-34.
49. Radi R. Peroxynitrite, a stealthy biological oxidant. *J Biol Chem* 2013; **288**: 26464-72.
50. Judee F, Simon S, Bailly C et al. Plasma-activation of tap water using DBD for agronomy applications: Identification and quantification of long lifetime chemical species and production/consumption mechanisms. *Water Res* 2018; **133**: 47-59.
51. Chauvin J, Judee F, Yousfi M et al. Analysis of reactive oxygen and nitrogen species generated in three liquid media by low temperature helium plasma jet. *Sci Rep* 2017; **7**: 4562.
52. Girard F, Badets V, Blanc S et al. Formation of reactive nitrogen species including peroxynitrite in physiological buffer exposed to cold atmospheric plasma. *RSC Advances* 2016; **6**: 78457-67.
53. Stokes JM, Lopatkin AJ, Lobritz MA et al. Bacterial Metabolism and Antibiotic Efficacy. *Cell Metab* 2019; **30**: 251-9.
54. Girotti AW. Photodynamic lipid peroxidation in biological systems. *Photochem Photobiol* 1990; **51**: 497-509.
55. Al-Sharify ZT, Al-Sharify TA, al-Azawi AM. Investigative study on the interaction and applications of plasma activated water (PAW). *IOP Conference Series: Materials Science and Engineering*, p. 012042, IOP Publishing.
56. Li Y, Pan J, Ye G et al. In vitro studies of the antimicrobial effect of non-thermal plasma-activated water as a novel mouthwash. *European journal of oral sciences* 2017; **125**: 463-70.
57. Su X, Feng M, Rogers S et al. The role of high voltage electrode material in the inactivation of E. coli by direct-in-liquid electrical discharge plasma. *Plasma Chemistry and Plasma Processing* 2019; **39**: 577-96.
58. Xiang Q, Kang C, Niu L et al. Antibacterial activity and a membrane damage mechanism of plasma-activated water against Pseudomonas deceptionensis CM2. *Lwt* 2018; **96**: 395-401.
59. Zhang Q, Liang Y, Feng H et al. A study of oxidative stress induced by non-thermal plasma-activated water for bacterial damage. *Applied physics letters* 2013; **102**.
60. Jyung S, Kang J-W, Kang D-H. L. monocytogens exhibited less cell membrane damage, lipid peroxidation, and intracellular reactive oxygen species accumulation after plasma-activated water treatment compared to E. coli O157:H7 and S. Typhimurium. *Food Microbiol* 2022; **108**: 104098.
61. Ischiropoulos H. Protein tyrosine nitration—an update. *Archives of biochemistry and biophysics* 2009; **484**: 117-21.
62. Lee J, Hunt JA, Groves JT. Manganese porphyrins as redox-coupled peroxynitrite reductases. *J Am Chem Soc* 1998; **120**: 6053-61.
63. Salgo M, Bermudez E, Squadrito G et al. Peroxynitrite causes DNA damage and oxidation of thiols in rat thymocytes [corrected]. *Archives of biochemistry and biophysics* 1995; **322**: 500-5.
64. Ferrer-Sueta G, Radi R. Chemical biology of peroxynitrite: kinetics, diffusion, and radicals. *ACS chemical biology* 2009; **4**: 161-77.
65. Nanni Jr EJ, Stallings MD, Sawyer DT. Does superoxide ion oxidize catechol,. alpha.-tocopherol, and ascorbic acid by direct electron transfer? *J Am Chem Soc* 1980; **102**: 4481-5.
66. Sawyer DT, Calderwood TS, Johlman CL et al. Oxidation by superoxide ion of catechols, ascorbic acid, dihydrophenazine, and reduced flavins to their respective anion radicals. A common mechanism via a combined proton-hydrogen atom transfer. *The Journal of Organic Chemistry* 1985; **50**: 1409-12.
67. Zheng H, Xu Y, Liehn EA et al. Vitamin C as scavenger of reactive oxygen species during healing after myocardial infarction. *International Journal of Molecular Sciences* 2024; **25**: 3114.
68. Yen G-C, Lai H-H. Inhibition of reactive nitrogen species effects in vitro and in vivo by isoflavones and soy-based food extracts. *J Agric Food Chem* 2003; **51**: 7892-900.